Magariyachi, T. [et al.]. Sound directivity by PT-symmetric acoustic dipoles. *Proc. SPIE 1769, Metamaterials XIII*, 117690P. DOI <10.1117/12.2593240>.

Sound directivity by $\mathcal{PT}$-symmetric acoustic dipoles

Tetsu Magariyachi[a,b], Helena Arias Casals[b], Ramon Herrero[b], Muriel Botey[b], and Kestutis Staliunas[b,c]

[a]Sony Corporation, 1-7-1 Konan, Minato-ku, Tokyo 108-0075, Japan
[b]Departament de Física, Universitat Politècnica de Catalunya (UPC), Colom 11, E-08222 Terrassa, Barcelona, Spain
[c]Institució Catalana de Recerca i Estudis Avançats (ICREA), Passeig Lluís Companys 23, E-08010, Barcelona, Spain

ABSTRACT

The new physics of open-dissipative, non-Hermitian systems have become a fruitful playground to uncover novel physical phenomena, even in exotic or counterintuitive ways, especially in optics and, more recently, also in acoustics. In this work, we propose a non-Hermitian metasystem in acoustics for the control of the sound field in two dimensions. The building blocks, or meta-atoms composing the arrangements, are pairs of identical Helmholtz resonators with different gain or loss functions. Such Helmholtz resonator dipoles may be designed to hold asymmetric scattering, as was theoretically analyzed and experimentally confirmed. Furthermore, aiming to create a complicated directivity, we explored different ensembles of Helmholtz resonator dipoles and numerically demonstrated a sound concentration with various configurations. The proposed non-Hermitian parity-time-symmetric dipoles made of a pair of Helmholtz resonators may be a potential artificial element for the creation of complex sound fields.

Keywords: Acoustic metamaterials, non-Hermitian acoustics, acoustic $\mathcal{PT}$-dipoles, Helmholtz resonators, sound directivity

1. INTRODUCTION

Non-Hermitian systems holding invariance under parity-time ($\mathcal{PT}$-) inversion have recently opened new horizons for the smart manipulation of waves.[1] An exceptional property of $\mathcal{PT}$-symmetric systems is the spontaneous breaking of the spatial symmetries, whereby the maximum asymmetry was achieved at the $\mathcal{PT}$-symmetry breaking point. Such space symmetry breaking occurs for potentials with specific spatial shifts between its real and imaginary parts, introducing asymmetric coupling between waves, i.e., a coupling directivity. In one-dimensional systems, symmetry breaking shows differences between right and left reflections, whereas for higher dimensionality, non-uniform directivity fields can be created. Discrete $\mathcal{PT}$-symmetric potentials can be generated by using spatially localized oscillators. In this way, $\mathcal{PT}$-symmetric lattices can be built as ensembles of asymmetric elements separated by subwavelength distances. The minimum system to break the space symmetry in a non-Hermitian manner is a $\mathcal{PT}$-symmetric dipole ($\mathcal{PT}$-dipole) showing asymmetric scattering.[2] Thus, a simple method of constructing $\mathcal{PT}$-symmetric metamaterials is to arrange individual $\mathcal{PT}$-dipoles, whose orientations can depend on their spatial position, to create the desired directivity field. In acoustics, asymmetric absorption has been demonstrated by detuned Helmholtz resonators (HRs) in a one-dimensional waveguide.[3] More recently, one- and two-dimensional arrays of HRs have been designed to achieve efficient sound absorption and diffusion.[4] Accordingly, a spatial distribution of HRs with modulated resonant frequencies and gain/loss can be feasible acoustic metamaterials analogous to those in optics[5] and microwave ranges.[6] Acoustic metamaterials can be generated using ensembles of HR dipoles, each one consisting of an amplifying and an attenuating HR.[7] The basic properties of such metamaterials would depend on the radiation properties of such HR dipoles, the building block of these non-Hermitian structures. In this paper, we experimentally demonstrate the asymmetric scattering of the non-Hermitian HR dipole in a two-dimensional space and also characterize the asymmetric frequency

Further author information: (Send correspondence to Tetsu Magariyachi)
Tetsu Magariyachi: E-mail: Tetsu.Magariyachi@sony.com, Telephone: +81 3 6748 2111

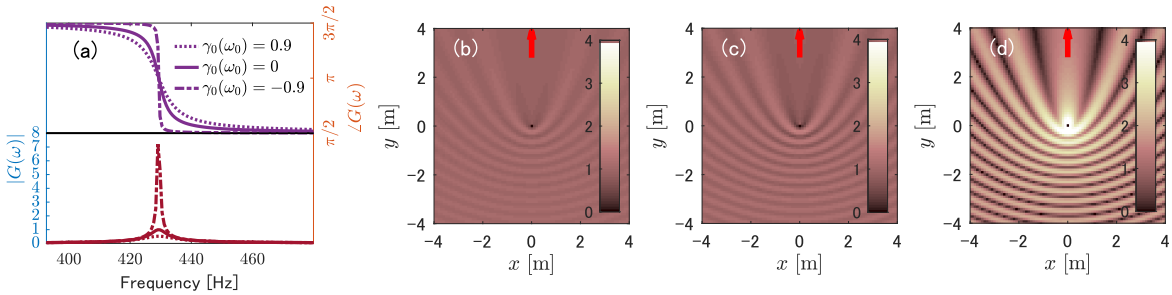

Figure 1. (color online) (a) Frequency responses, gain function $G(\omega)$, of a single HR with loss (dotted curve), neither loss nor active gain, neutral (solid curve), and gain (dashed curve). Negative (positive) loss factors $\gamma_0(\omega_0)$ correspond to active gain (active losses) generating peak amplitudes at higher (lower) than 1 with sharper (smoother) phase shifts. (b–d) Total pressure field created by the incident plane wave and the scattered wave from (b) loss, (c) neutral, and (d) gain HR at the origin. Source frequency is $f = 429.1$ Hz, corresponding to the peak of the gain functions. Fringes are observed around the HR, indicating interference between the incident and scattered fields. The parameters were set as follows: $a = 2$ mm (radius of HR neck cross section), $d = 20$ mm (height of 2D field), $l' = 13.07$ mm (corrected length of HR neck), $f_0 = 436.3$ Hz (resonant frequency of HR in 1D), and $c = 340$ m/s (sound velocity).

response. Results meet a good agreement with the developed theoretical analysis. Different arrangements of HR dipoles are designed to achieve sound manipulation effects of sound concentration.

2. SCATTERING AND COUPLING PROPERTY OF HR DIPOLE IN 2D SPACE

2.1 Scattering property of single HR

The scattered acoustic pressure from one HR in a 2D field when an input pressure field P_{in} is applied is expressed as a function of the position from resonator r and the angular frequency ω given by $P_{scat}(\vec{r},\omega) = H_0^{(2)}(kr)G(\omega)P_{in}(\omega)$, where $H_0^{(2)}$ denotes the 0th order Hankel function of the 2nd kind and $G(\omega)$ denotes the gain function, expressed as $G(\omega)^{-1} = G_0^{-1}(\omega) - 1 - i\frac{2}{\pi}\ln\left(\frac{2}{\epsilon ka}\right)$, with $G_0(\omega)^{-1} = i\gamma_{c2}^{-1}\left(\frac{\omega_0^2}{\omega^2} - 1\right) - \gamma_0(\omega)$, where ω_0, k, $\gamma_{c2} = S_h/4dl'$, and $\gamma_0(\omega) = \gamma/\gamma_{c2}\omega$ denote the resonant angular frequency, the wave number, the coupling loss factor in 2D, and the relative loss factor of the HR. d denotes the thickness of the 2D field, l' the corrected HR neck length, S_h the cross section of the HR neck, and γ the loss factor of the HR. Unless otherwise noted, hereafter, we omit "ω" from G, P_{scat}, and P_{in} for brevity.

The frequency responses of G for different relative loss factors are depicted in Fig. 1(a) HR with loss, neutral HR (without gain nor loss), and HR with gain, with the relative loss factors of $\gamma_0(\omega_0) = 0.9$, 0, and -0.9, respectively. We can observe the peak of G amplitude at unity for a neutral HR, whereas those for the HR with loss and gain are observed at lower and higher values. The phases change from $3\pi/2$ to $\pi/2$ through π at around the peak frequency and the transition is milder for loss HR and steeper for gain HR. Figures 1(b–d) illustrate the total pressure field, i.e., the scattered and the incident waves, with these three HRs placed at the origin when the plane wave is arriving from the bottom and progressing to the top, as indicated by the red arrow. The calculated pressure is normalized by incident pressure. We observe the scattering from the HR as interference fringes and how they become sharper as the gain becomes larger.

2.2 Scattering property of HR dipole

Contrary to the homogeneous scattering obtained from the single HR, when HRs are placed close to each other, the scattering P_{scat} holds directivity depending on the source and measurement positions $\vec{r_s}$ and $\vec{r_m}$:

$$P_{scat}(\vec{r_s},\vec{r_m}) = \boldsymbol{h_m}(\vec{r_m})^{\mathrm{T}}\tilde{\boldsymbol{G}}\boldsymbol{h_s}(\vec{r_s})P_0, \tag{1}$$

with $\tilde{\boldsymbol{G}} = \boldsymbol{(I - GH_0)^{-1}G}$, where $\boldsymbol{h_m}(\vec{r_m}) = \{H_0^{(2)}(k|\vec{r_m} - \vec{r_1}|), \cdots, H_0^{(2)}(k|\vec{r_m} - \vec{r_N}|)\}^{\mathrm{T}}$ and $\boldsymbol{h_s}(\vec{r_s}) = \{H_0^{(2)}(k|\vec{r_1} - \vec{r_s}|), \cdots, H_0^{(2)}(k|\vec{r_N} - \vec{r_s}|)\}^{\mathrm{T}}$ denote the 2D field propagation from HRs to the measurement points and from a source to HRs, respectively. $\vec{r_n}$ denotes the position of the nth HR out of N, $\boldsymbol{G}$ denotes the diagonal matrix

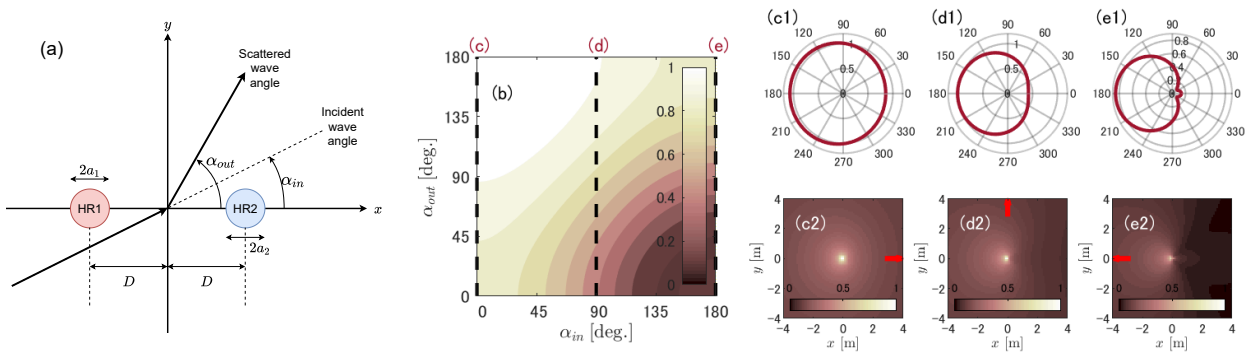

Figure 2. (color online) (a) A schematic to explain the variables and parameters of the dipole. (b) Multistatic matrix, i.e., the dependence of scattering on incidence angle α_{in} and observation angle α_{out}. The source frequency is $f = 432$ Hz, $D = 0.05$m, and $r_s = r_m = 100$m; the rest of the parameters are the same as in Fig. 1. Note that owing to symmetry, only 1/4 of the map is plotted (other quadrants can be obtained as mirror symmetries). (c1–e1) Polar plots of directivity and (c2–e2) scattered pressure fields for several incidence angles (which are the vertical cross sections at the dotted lines in (b)).

having the value of the nth HR gain G_n for the nth diagonal element, and $\boldsymbol{H_0}$ represents the decay functions between the HRs and has the value $H_0^{(2)}(k|\vec{r_n} - \vec{r_{n'}}|)$ for the (n, n')th element. We formed the $\mathcal{PT}$-dipole consisting of two HRs having loss/gain properties $\gamma_0(\omega_0) = \pm 0.9$ and located close to each other, as depicted in Fig. 2(a), and calculated the multistatic matrix, $\bar{G}(\alpha_{in}, \alpha_{out})$, which represents the scattering gain property of the dipole for every incident (α_{in}) and scattered (α_{out}) angle. $|\bar{G}(\alpha_{in}, \alpha_{out})|$ is calculated by normalizing $P_{scat}(\vec{r_s}, \vec{r_m})$ with P_0, $|H_0^{(2)}(kr_s)|$, and $|H_0^{(2)}(kr_m)|$, i.e., the source amplitude, and decays from the source to the origin and from the origin to the measured point, respectively. In Fig. 2(b), the amplitude of the multistatic matrix is illustrated for the frequency $f = 432$ Hz, where the horizontal and vertical axes represent the incident and scattered angles, respectively. Distances from the HR dipole to the source and to the measured point are fixed as $r_s = r_m = 100$m. Figure 2(b) consists of the polar pattern of scattering from each incident angle, α_{in}, where some of them are shown in Figs. 2(c1–e1) for $\alpha_{in} = 0, 90$, and $180°$. Because of the reciprocity law and the symmetric configuration around the x-axis, symmetry is observed around the diagonal axis $\alpha_{in} + \alpha_{out} = 180°$. In contrast, strong asymmetry is observed around the diagonal line $\alpha_{in} = \alpha_{out}$, where the tendency is also noticable in the gradual attenuation of backward scattering from Figs. 2(c) to (e).

Since our goal is to create directivity regardless of the incident wave direction, the tendency of the overall scattered wave was calculated by averaging the power of the multistatic matrix over the incident angle. We call this tendency integral directivity (ID) and it is defined as follows:

$$\mathrm{ID}(\alpha_{out}) = \frac{1}{2}\int_0^{2\pi} |\bar{G}(\alpha_{in}, \alpha_{out})|^2 d\alpha_{in}. \tag{2}$$

This allows us to plot the directivity pattern of scattering from the dipole for the whole incident wave. In addition, in order to observe the tendency of the directivity in frequency domain, deflection $D_{RL}(f)$ was calculated using

$$D_{RL}(f) = 10 \ln\left(\frac{\mathrm{ID}_R(f)}{\mathrm{ID}_L(f)}\right) \tag{3}$$

with $\mathrm{ID}_L = \frac{1}{\pi}\int_{\pi/2}^{3\pi/2} \mathrm{ID}(\alpha_{out}) d\alpha_{out}$ and $\mathrm{ID}_R = \frac{1}{\pi}\int_{-\pi/2}^{\pi/2} \mathrm{ID}(\alpha_{out}) d\alpha_{out}$. $D_{RL}(f)$ represents the amount of scattered energy to the right-hand side relative to the left one in dB. The positive and negative values of ID correspond to the deflections to the right and the left, respectively. Figure 3(a) depicts the deflection as a function of frequency and (b1,c1) depict the ID for the frequencies corresponding to the dashed lines in (a). ID is close to zero at low frequencies and increases as the frequency approaches that at (b), which has the maximum ID to the right. Then, ID drops sharply, crossing 0 dB at around the peak frequency of $|G|$, and flips to the left side. The frequency at

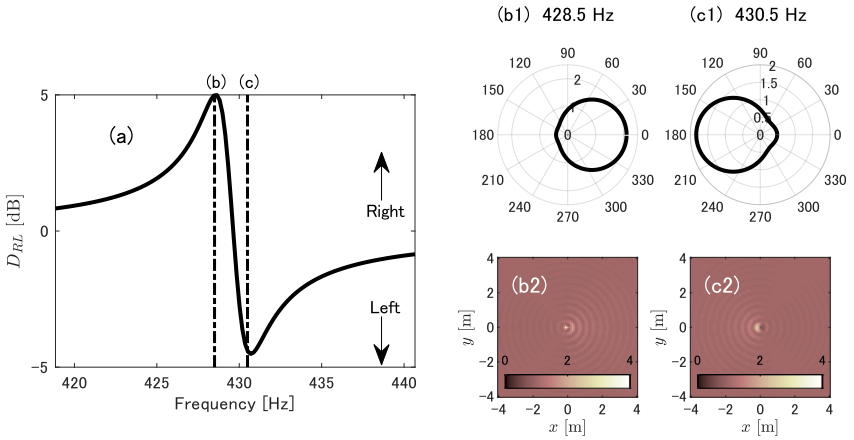

Figure 3. Integrated directivity (ID) depending on frequency. (a) Intensity deflection in decibels (dB) as a function of frequency. (b1,c1) Integrated directivity in polar coordinates and for frequencies corresponding to the vertical dashed lines in (a). (b2,c2) Total normalized intensity fields averaged over the incident wave angle α_{in} every five degrees.

point (c) is close to the one used in Fig. 2, where the deflection has a maximum to the left. As the frequency further increases, ID converges to zero. Figures 3(b2,c2) illustrate the total intensity field normalized by the intensity of the incident wave and that averaged over the incident wave angle every five degrees. From these figures, we can confirm the directivity to the right and the left, respectively, for the corresponding frequencies.

3. EXPERIMENTAL EVALUATION WITH PASSIVE NON-HERMITIAN DIPOLE

We conducted an experiment to confirm the asymmetric scattering property of the non-Hermitian HR dipole in a 2D field, using HRs with the same geometric features, but one is neutral, i.e., no loss/gain, and the other has loss. The setup of the experiment and the HRs are shown in Figs. 4(a–c), where (a) is the top view of the 2D field, (b) is the schematic of the cross section from a side, and (c1,c2) are neutral and loss HRs. The scattering $P_{scat}(\alpha_{in}, \alpha_{out})$ was obtained by measuring the total pressure $P(\alpha_{in}, \alpha_{out})$ with the HRs attached to the 2D field, and then subtracted by the incident pressure $P_0(\alpha_{in}, \alpha_{out})$ measured without HRs. The source and measured positions were set from 0 to 180° in 30° intervals, with the radii of $r_s = 130$mm and $r_m = 110$mm. The multistatic matrix was calculated by normalizing $P_{scat}(\alpha_{in}, \alpha_{out})$ with the incident pressure $P_0(0, 0)$ (to compensate system characteristics) and the decays, $|H_0^{(2)}(kr_s)|$ and $|H_0^{(2)}(kr_m)|$, i.e., from the source to the origin and from the origin to the measure point, respectively. For the evaluation of the result, we calculated theoretical values for the multistatic matrix and the deflection exploiting the aforementioned formulas. The parameters needed in the calculation, i.e., loss factors, γs and ω_0s, were determined in a pre-experiment conducted in a 1D waveguide.[7] Figure 4(d) depicts the frequency response of the deflection of the dipole by the theoretical calculation (black solid line) and from the experimental results (red dashed line). The multistatic matrices for two frequencies 743 Hz and 810 Hz are shown in Figs. 4(e,g) and (f,h), respectively, where (e,f) are those of the experimental result and (g,h) are those of the theoretical calculation. For the frequency of 743 Hz, both (e) and (g) show greater amplitude toward the bottom-right side compared with the top left, i.e., scattering is to the right side. For the frequency of 810 Hz (f,h), in contrast, the top-left sides indicate greater amplitude, i.e., scattering is to the left side. The comparison shows the good agreement for both the deflection and the multistatic matrices. This result confirms the asymmetric scattering of a passive non-Hermitian HR dipole in 2D and thus, also ensures the validity of the effect for the $\mathcal{PT}$-HR dipole with gain.

4. SOUND CONCENTRATION WITH ENSEMBLES OF $\mathcal{PT}$-HR DIPOLES

The HR dipoles, with the specific characteristics discussed in the previous section, can be used as building blocks of a more complex metastructure. It is known that the continuous PT-media can serve as wave concentrators.[8,9] Here, we propose that the ensemble of PT-dipoles can also be used. Such configurations are expected to concentrate the sound arriving from arbitrary angles to one spot. We demonstrate three configurations that realize

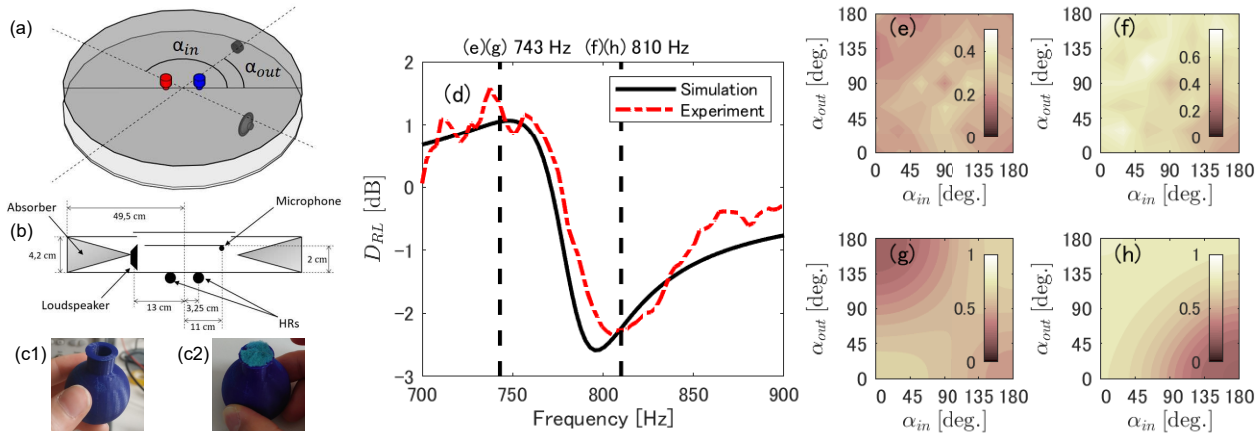

Figure 4. (color online) Experimental setup and the results. (a) Schematic of the experimental setup. (b) Geometry of the setup in the cross-section viewpoint. The parameters are $a = 5$ mm, $d = 20$ mm, $D = 32.5$ mm, $f_0 = 820$ Hz, $l' = 17.21$ mm, $r_m = 110$ mm, $r_s = 130$ mm, $\gamma_0(\omega_0) = 0$ (neutral), and $\gamma_0(\omega_0) = 1.535$ (loss). (c1,c2) The neutral and loss HRs used in the experiment, where the entrance of the loss HR is covered with a slice of sponge. (d) Experimental result (red dashed line) and result of the theoretical calculation (black solid line) for deflection analysis. (e,f) Multistatic matrices of the experimental result for the frequencies of 743 Hz and 810 Hz, respectively. (g,h) Multistatic matrices of the theoretical calculation for the same frequencies as (e,f).

such concentration. The first configuration is shown in Figs. 5(a,b), where ten dipoles are aligned vertically and every dipole directs the gain toward $(x, y) = (-2, 0)$ and thus tilted toward the horizontal axis $y = 0$ to form the focus. For comparison, we also consider the case where the tilt is directed outward (c,d).

In this configuration, the intensity fields were calculated for the incidence of a plane wave from many directions. The intensity fields are normalized by the intensity at origin without HRs, calculated for every incident direction (every 5 degrees) and averaged over all incident angles. The results are shown in Figs. 5(b,d). A significant focus is clearly shown in (b) in contrast to (d). The second configuration (Figs. 5(e,f)) uses the same dipoles and source frequency as the previous one, but they are distributed in a half-circle, with its gain HRs directed inside the circle. High concentration can be observed inside the half-circle. By contrast, no concentration is observed when gain and loss are flipped (Figs. 5(g,h). The third configuration (Figs. 5(i,j)) has the same HR geometry but the gain HR is replaced by a neutral one. Furthermore, the source frequency is slightly different (431.0 Hz), as the peak frequency of the deflection shifts with the change of the gain factor. This configuration forms a full-circle array of dipoles and it is the passive version of the one demonstrated in [7] with a high concentration. The result also shows the high concentration compared with the version of flipped dipoles (Figs. 5(k,l)). This interesting result indicates that passive HR dipoles can also create such sound concentrations.

5. CONCLUSION

We proposed acoustic $\mathcal{PT}$-dipoles in two dimensions, composed of two HRs having identical geometry but opposite loss factors, with strong directivity in a scattered wave field, and its use as building blocks of metastructure, that enables sound field control. The spatial scattering characteristics of the HR dipole for the incident wave were obtained using analyses of the multistatic matrix and integral directivity and showed the expected asymmetric scattering in 2D. Moreover, the total normalized intensity field for the dipoles was calculated to confirm the asymmetric scattering in the 2D field. The asymmetric scattering from such HR dipoles was demonstrated in a 2D experiment, where the non-Hermitian HR dipole was formed of a neutral HR and a HR with loss. The experimental results and the analytical predictions directly showed good agreement. Finally, we explored the assemblies of such dipoles to design a metastructure for the control of the sound flow. Several configurations of the dipole arrangement demonstrated good sound concentration performance. Indeed, a sound field concentration in 2D was predicted for the use of a circular arrangement of passive $\mathcal{PT}$-symmetric HR dipoles. The result

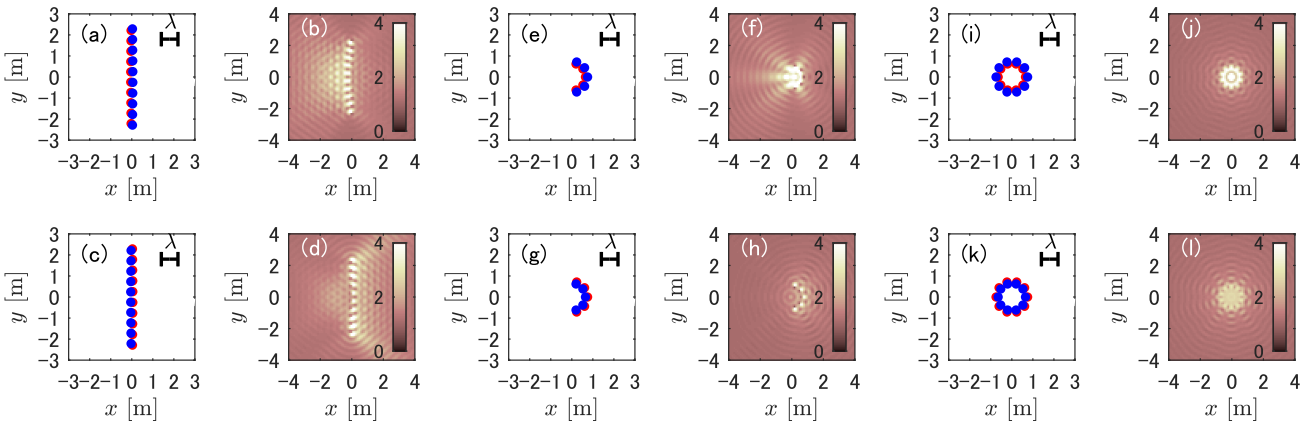

Figure 5. (color online) Fields and field flows in an ensemble of HR dipoles. (a,c) Vertical distributions of HR dipoles in a 2D field, where in (a) the gain of the dipole is directing to the point $x = -2$ on the x-axis and in (c) the loss/gain are flipped. (b,d) show respectively the normalized intensity field averaged over the incident angle (every 5°) for both distributions (a,c) for a frequency of $f = 430.5$ Hz. (e,g) Dipole configuration in a half circle array where the gains of the dipoles are inside the circle in (e) and opposite in (g). (i,k) are the circular configuration of the HR dipoles with the identical geometric feature as the previous ones, with different gain property $\gamma_0(\omega_0) = 0$ (the loss is the same $\gamma_0(\omega_0) = 0.9$). (f,h,j,l) Averaged intensity fields, calculated the same as (b,d).

.

of this study may provide a new platform for several applications for creating nontrivial sound field propagation control based on $\mathcal{PT}$-symmetry breaking.

ACKNOWLEDGMENTS

The work is partially supported by Sony Corporation and by Spanish Ministerio de Ciencia e Innovación (PID2019-109175GB-C21).

REFERENCES

[1] Jackson, J. D., [*Classical Electrodynamics*], John Wiley and Sons, 3rd Edition ed. (1998).

[2] Staliunas, K., Markoš, P., and Kuzmiak, V., "Scattering properties of a $\mathcal{PT}$ dipole," *Phys. Rev. A* **96**, 043852 (Oct 2017).

[3] Long, H., Cheng, Y., and Liu, X., "Asymmetric absorber with multiband and broadband for low-frequency sound," *Appl. Phys. Lett.* **111**, 143502 (Oct. 2017).

[4] Herrero-Durá, I., Cebrecos, A., Picó, R., Romero-García, V., García-Raffi, L. M., and Sánchez-Morcillo, V. J., "Sound absorption and diffusion by 2D arrays of Helmholtz resonators," *Appl. Sci.* **10**, 1690 (Mar. 2020).

[5] Medina Pardell, J., Herrero, R., Botey, M., and Staliunas, K., "Stabilized narrow-beam emission from broad-area semiconductor lasers," *Phys. Rev. A* **101**, 033833 (Mar 2020).

[6] Chen, T., Tang, W., Mu, J., and Cui, T. J., "Microwave metamaterials," *Ann. Phys.* **531**, 1800445 (Apr. 2019).

[7] Magariyachi, T., Arias Casals, H., Herrero, R., Botey, M., and Staliunas, K., "$\mathcal{PT}$-symmetric Helmholtz resonator dipoles for sound directivity," *Phys. Rev. B* **103**, 094201 (Mar 2021).

[8] Ahmed, W. W., Herrero, R., Botey, M., Hayran, Z., Kurt, H., and Staliunas, K., "Directionality fields generated by a local Hilbert transform," *Phys. Rev. A* **97**, 033824 (Mar 2018).

[9] Hayran, Z., Herrero, R., Botey, M., Kurt, H., and Staliunas, K., "Invisibility on demand based on a generalized Hilbert transform," *Phys. Rev. A* **98**, 013822 (Jul 2018).